Electronic Supplementary Information

Luminescent Single-molecule Magnet: Observation of Magnetic Anisotropy Using Emission as Probe.

Kei Yamashita, Rie Miyazaki, Yumiko Kataoka, Takayuki Nakanishi, Yasuchika Hasegawa,*
Motohiro Nakano, Tomoo Yamamura, and Takashi Kajiwara*

Synthesis of 1: $[Zn(L)]\cdot 2H_2O$ was obtained as previously described (Costes, J.-P.; Laussac, J.-P.; Nicodème, F. J. *Chem. Soc., Dalton Trans*. **2002**, 2731). A solution of $[Zn(L)]\cdot 2H_2O$ (0.1 mmol) in 1:1 methanol/acetone (1 mL) was combined with 0.1 mM methanolic solution of $Tb(NO_3)_3\cdot 5H_2O$ (0.5 mL , 0.05 mmol) and 0.1 mM methanolic solution of tetrabutylammonium bromide (1 mL, 0.1 mmol). The addition of 0.1 mM methanolic solution of tetraphenylborate sodium salt (0.5 mL, 0.05 mmol) to the combined solution gave yellow crystals after several days. Crystals were filtered off and dried in vacuo yielding about 70 %. The composition of the freshly prepared crystal was estimated to be $\mathbf{1}\cdot 2MeOH\cdot$acetone via X-ray analysis. Crystals slowly release crystallization solvent molecules to give $\mathbf{1}\cdot n$MeOH ($n < 1$), which was confirmed by thermogravimetric analysis (Fig. S1), and the drying process was completed after heating to 100 ^{o}C which resulted into **1**. This dried sample adsorbs atmospheric water to generate $\mathbf{1}\cdot 2H_2O$. The sample used for elemental analysis was dried in the vacuum condition for 0.5~1.0 h at room temperature, and the sample was stored in the air: hence the expected composition of the sample is non-stoichiometric for solvent molecules which is given as $\mathbf{1}\cdot m\mathrm{MeOH}\cdot n\mathrm{H_2O}$ ($m < 1$, $n < 2$). Elemental analysis [%] calcd for $\mathbf{1}\cdot 0.5MeOH\cdot 1.5H_2O$ C 51.29; H4.91; N 3.54. Found C 51.20; H 5.24; N 3.54.

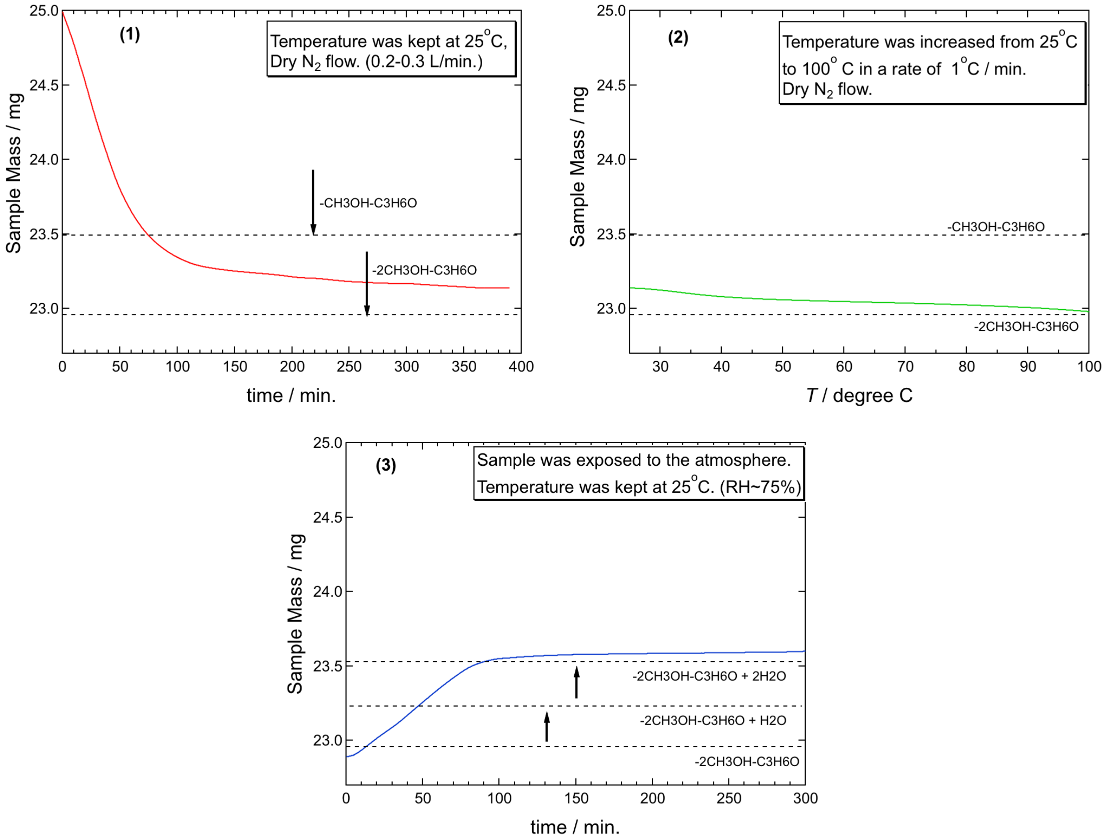

Fig. S1. Thermogravimetric analysis of a freshly prepared sample of **1**·2MeOH·acetone. Weight variation was first measured in flowing dry N_2 gas (1 and 2), and then in the air (3). The temperature was maintained at 25°C during the first measurement (1), then increased to 100 $^{\mathrm{o}}$C with the rate of 1$^{\mathrm{o}}$C / min (2), and cooled to 25 $^{\mathrm{o}}$C and maintained at this temperature (3). The sample quickly desorbs the acetone molecule and one methanol molecule in the first process. The rest methanol molecule is slowly released under heating, and it is completed in several hours. The dried sample quickly absorbs moisture from the air when the sample was exposed to the atmosphere.

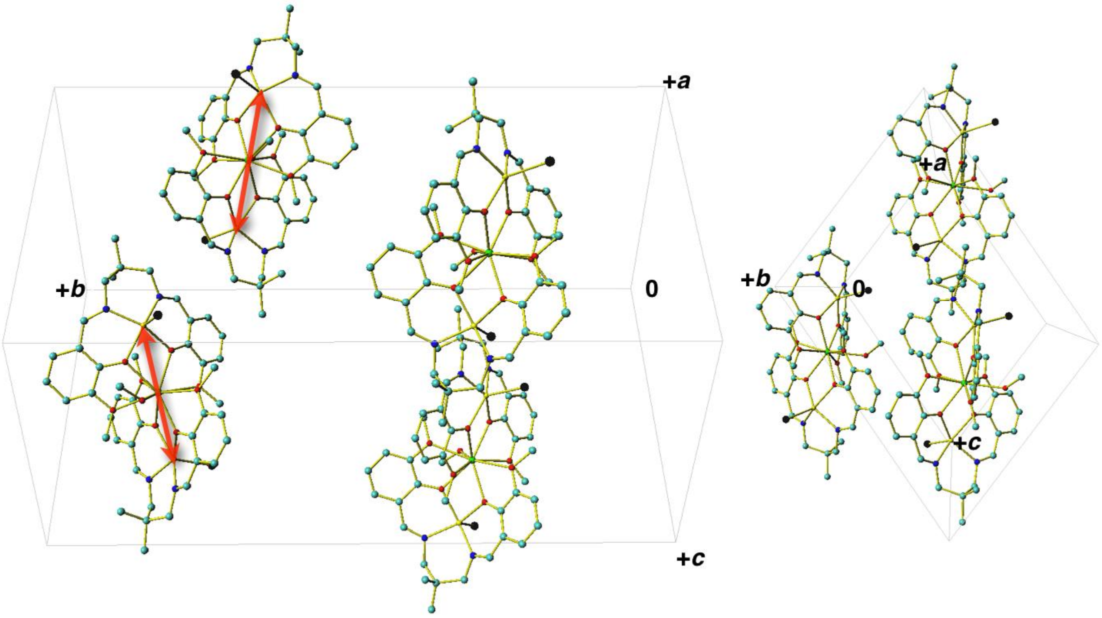

Fig. S2 Packing diagrams of the cationic part of **1**. Hydrogen atoms are omitted for clarity. Green Tb^{III}, yellow Zn^{II}, red O, black Br, blue N, light blue C. The unit cell of **1**·2MeOH·acetone includes four molecules in two different orientations, which are correlated by a crystallographic 2_1 axis parallel to the *b*-axis. Red arrows in the left Fig. represent the Zn^{II}-Tb^{III}-Zn^{II} axis in each molecule, which would be correlated with the principal axes. The angle between two tilting arrows was estimated as *ca*. 24º.

Solid state luminescent spectra of 1: Complex **1** in the solid state showed an efficient f-f emission even at room temperature upon irradiation of UV light at 380 nm, with emission quantum yield estimated as 11% at 300 K. The emission spectra were collected in the temperatures range of 77ï 300 K, which is shown below.

a) 300 K

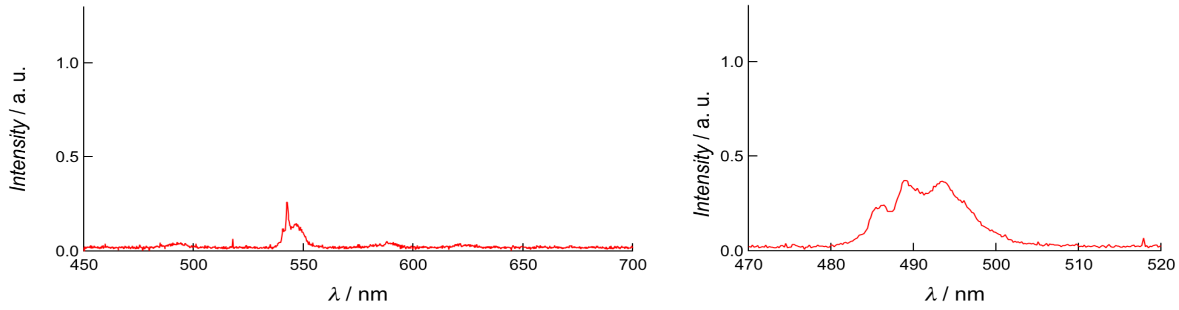

b) 200 K

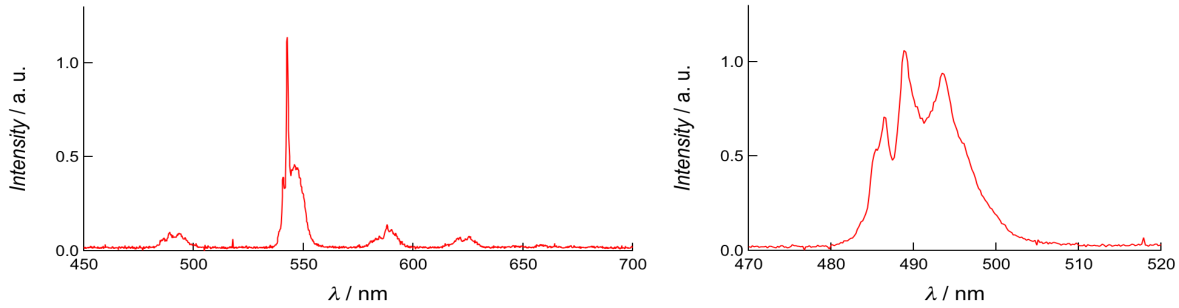

c) 100 K

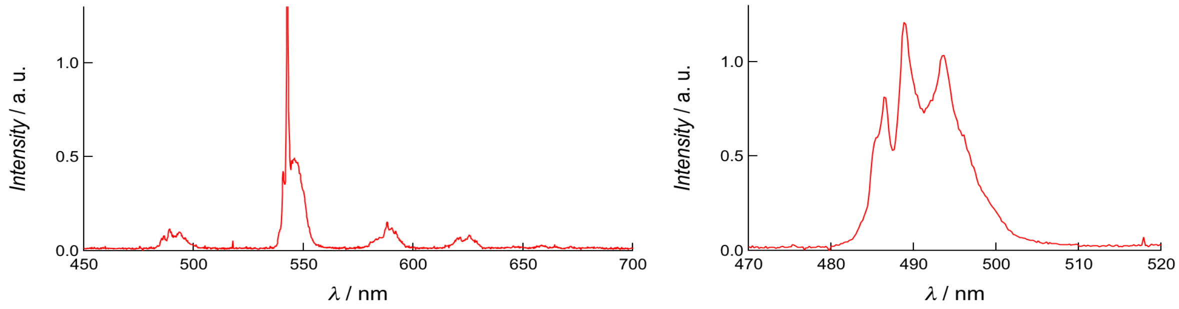

d) 77 K

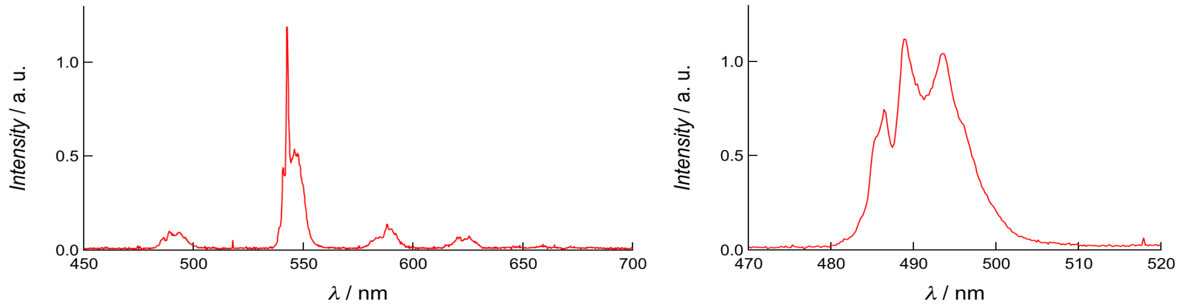

Fig. S3 Temperature dependence of the emission spectra of the slide state **1** measured by the irradiation at 380 nm.

Magnetic properties: Magnetic susceptibility measurements were performed using Quantum Design magnetometer PPMS-9 and MPMS-5S. The mixture of the powdered sample and eicosane was cooled to 2 K, and dc field was applied up to 9 T during which the magnetization saturation was monitored. Once the sample was aligned along the field, it was first heated to 320 K to melt the eicosane and then cooled to 300 K to fix the crystals aligned along the principal axis. The dc measurements were performed over the temperature range 2.0ï 300 K with the 1000 Oe dc field applied. Diamagnetic corrections for the samples were determined from Pascalôs constants. Ac measurements were performed at various frequencies from 10 to 10000 Hz with oscillating field amplitude of 3 Oe and external dc fields (H_{ex}) of 0, 500, or 1000 Oe.

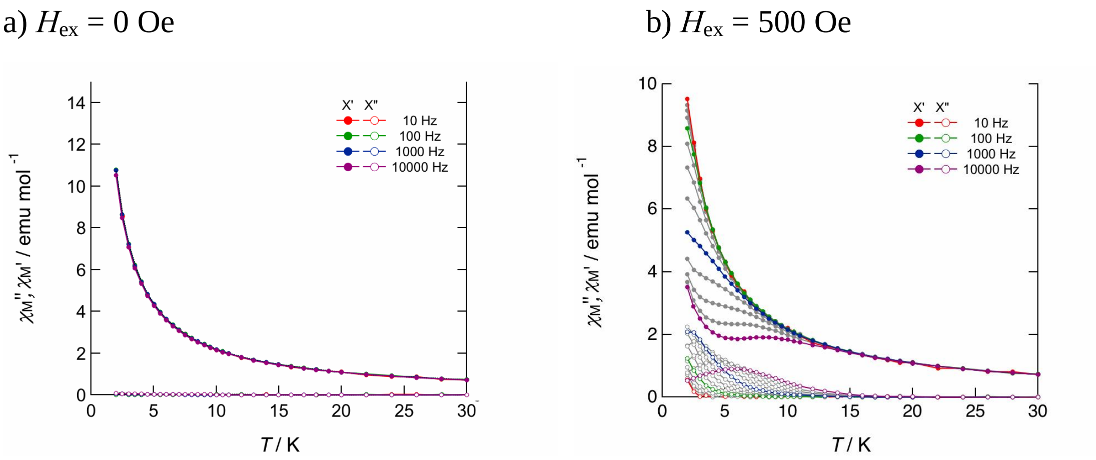

a) H_{ex} = 0 Oe

b) H_{ex} = 500 Oe

c) H_{ex} = 1000 Oe

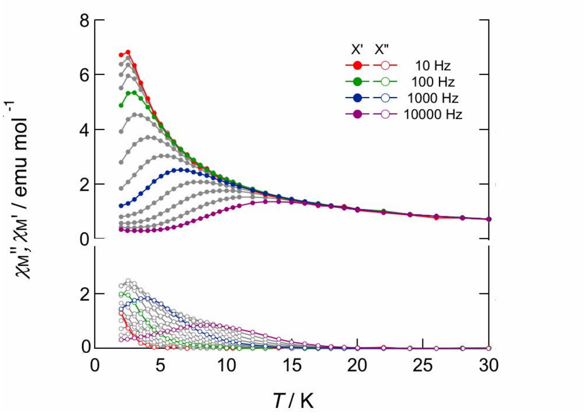

Fig. S4 Temperature dependence of the in-phase (closed circles) and out-of-phase (open circles) components of ac susceptibility data of **1** measured under 0, 500, and 1000 Oe dc fields.

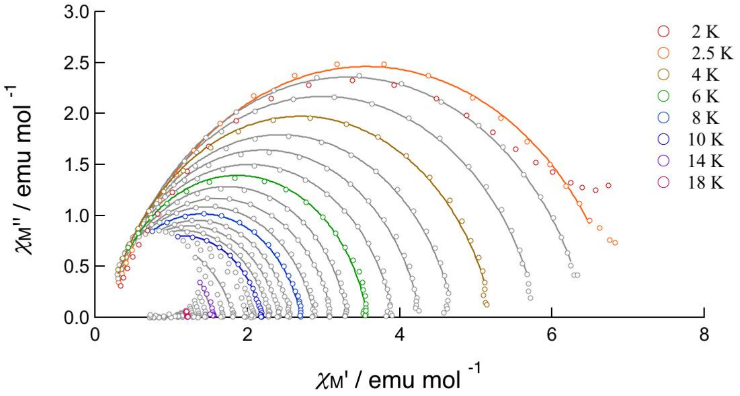

Fig. S5 Cole-Cole analyses of **1** for the data measured under 1000 Oe dc field. Solid curves are the best fitting calculations. α values were estimated as 0.218 (2.5 K), 0.199 (3.0 K), 0.184 (2.5 K), 0.172 (4.0 K), 0.167 (4.5 K), 0.157 (5.0 K), 0.159 (5.5 K), 0.140 (6.0 K), 0.141 (6.5 K), 0.171 (7.0 K), 0.179 (7.5 K), 0.171 (8.0 K), 0.169 (8.5 K), 0.188 (9.0 K), 0.199 (9.5 K), and 0.176 (10.0 K), respectively.

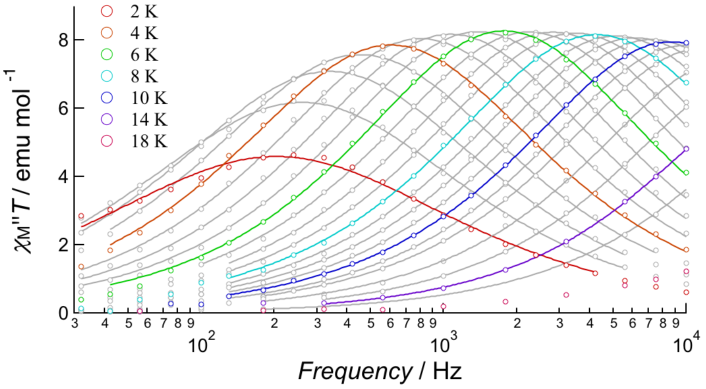

Fig. S6 Frequency dependence of the $\chi_M''T$ products which were analyzed by the generalized Debye model. Solid curves are the best fitting calculations. α values were estimated as 0.204 (2.5 K), 0.182 (3.0 K), 0.173(3.5 K), 0.167 (4.0 K), 0.158 (4.5 K), 0.152 (5.0 K), 0.148 (5.5 K), 0.150 (6.0 K), 0.159 (6.5 K), 0.157 (7.0 K), 0.156 (7.5 K), 0.157 (8.0 K), 0.156 (8.5 K), 0.152 (9.0 K), 0.145 (9.5 K), and 0.149 (10.0 K), respectively.

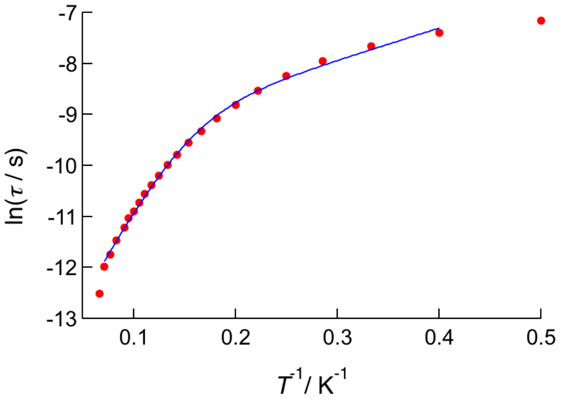

Fig. S7 Arrhenius plot for complex **1** measured under 1000 Oe external field. The solid curve is a theoretical calculation corresponding to Christou's formula, with two sets of the kinetic parameters as τ_0 = 5.5(8) × 10^{-5} s and ΔE = 6.3(5) K for the lower barrier and τ_0 = 5.6(7) × 10^{-7} s and ΔE = 36(1) K for the higher barrier.

Determination of the magnetic anisotropy parameters from the dc susceptibility data: Field dependence of the magnetization was measured at 2.0 K, for the field-aligned sample of **1** with the magnetic fields applied along the magnetic easy-axis (Fig. S8). If the Tb^{III} ion has a strong easy-axis anisotropy, it behaves as an Ising spin at low temperatures with the J_z value of ±J. The saturated magnetization $M_S/N\mu_B$ could be represented as $g_J|J_z| = g_J J$ when the principal axis of the microcrystals was aligned along the magnetic field, and the expected saturated magnetization is calculated as 9.0 $N\mu_B$ for **1**. The observed magnetization is smaller than the expected values because of the deviation from the complete alignment. Using θ, which is defined as the averaged angle between the field and principal axis of each molecule, saturated magnetizations are represented as $g_J J\cos\theta$, and from the value of saturation at 5.0 T, θ is roughly estimated as 30°. The solid line in Fig. S8 is a theoretical curve calculated on the basis of the anisotropic spin Hamiltonian (see below) with the θ value of 29°. Incomplete alignment of crystals of **1** showing a relatively large θ value might be due to the tilted alignment of the molecules in the crystal described above, which was estimated as *ca*. 24° (see Fig. S2).

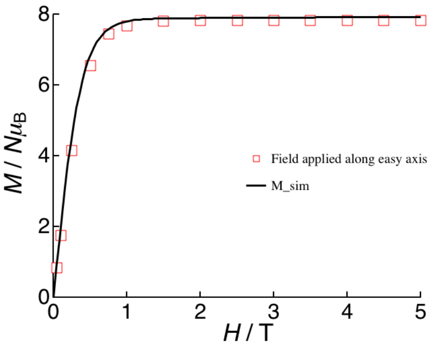

Fig. S8 Field dependence of the magnetization measured at 2.0 K, measured for the field-aligned sample of **1** with the magnetic fields applied along the magnetic easy-axis. The solid curve is a theoretical calculation using the magnetic anisotropy parameters and tilting angle θ given below.

The temperature dependence of the $\chi_M T$, shown in Fig. S9 below, was roughly analyzed by using the anisotropy Hamiltonian in Equation 1:

$$\hat{H} = B_2^0 \hat{O}_2^0 + B_4^0 \hat{O}_4^0 + B_6^0 \hat{O}_6^0 \quad (1)$$

accompanied by the Zeeman effect term. B_n^0's are axial anisotropy coefficients of n-th order and $\hat{O}_n^0$ denotes the corresponding Stevensô operator equivalents (Schmitt, D. *J. Physique* **1986**, *47*, 677; Sievers, J. *Z. Phys. B Cond. Matter* **1982**, *45*, 289). In the analysis, the averaged angle θ between the applied magnetic field and the principal axis of each molecule was fixed at observed value, 30°, at the first cycle of the least square fitting, and then it was included as a fitting parameter. Depending on the initial values of B_n^0's, several sets of best-fit values of (B_2^0/k_B, B_4^0/k_B B_6^0/k_B) were obtained showing similar analytical errors, and one of the best theoretical curves was shown in Fig. S9 which was calculated for the parameter set of (B_2^0/k_B, B_4^0/k_B B_6^0/k_B) = (ï 5.6 K, 0.0071 K, ï 0.00044 K) with the averaged angle θ of 29.8°. The energy diagram for the ground multiple of $^7F_6$ was estimated from these B_n^0 parameters which is shown in Fig. S10. In this study, only axial terms were included in the Hamiltonian which resulted in a good agreement with the observed data. The contribution of the rhombic terms might not be dominant, however, introduction of the terms such as B_2^2 would lead to better precision of the fitting between theoretical curve and the observed data. To avoid the overparametrization, further investigation would not be given in this study.

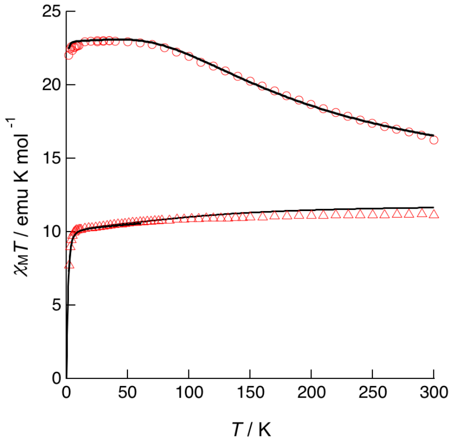

Fig. S9 The temperature dependence of the $\chi_M T$ products measured for field-aligned sample (o) and randomly oriented sample (Δ) of **1** with the 1000 Oe dc field, with the field applied along the magnetic easy-axis for the former. Solid curves represent the theoretical calculations.

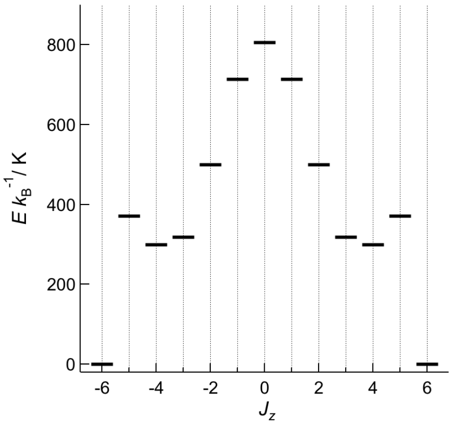

Fig. S10 Energy level diagram of J_z sublevels estimated from magnetic anisotropic parameters of (B_2^0/k_B, B_4^0/k_B B_6^0/k_B) = (ï 5.6 K, 0.0071 K, ï 0.00044 K).

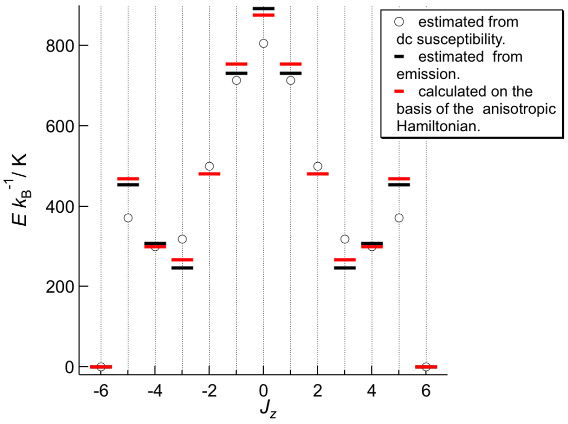

Fig. S11 Summarized energy level diagram of J_z sublevels estimated from the emission fine structure (—) and the calculation on the basis of the anisotropic Hamiltonian (see main text) with magnetic anisotropic parameters of (B_2^0/k_B, B_4^0/k_B B_6^0/k_B) = (ï 5.4 K, 0.0080 K, ï 0.00063 K) (—).

The energy levels estimated from the dc susceptibility measurement were also given (o), which were estimated with the magnetic anisotropic parameters of (B_2^0/k_B, B_4^0/k_B B_6^0/k_B) = (ï 5.6 K, 0.0071 K, ï 0.00044 K).